

**Molecular simulations of self-assembly processes in metal-organic frameworks:
Model dependence**

Debasmita Biswal and Peter G. Kusalik

Citation: [The Journal of Chemical Physics](#) **147**, 044702 (2017); doi: 10.1063/1.4994700

View online: <http://dx.doi.org/10.1063/1.4994700>

View Table of Contents: <http://aip.scitation.org/toc/jcp/147/4>

Published by the [American Institute of Physics](#)

**COMPLETELY
REDESIGNED!**



**PHYSICS
TODAY**

Physics Today Buyer's Guide
Search with a purpose.

Molecular simulations of self-assembly processes in metal-organic frameworks: Model dependence

Debasmita Biswal and Peter G. Kusalik^{a)}

Department of Chemistry, University of Calgary, 2500 University Dr. NW, Calgary, Alberta T2N 1N4, Canada

(Received 13 March 2017; accepted 6 July 2017; published online 25 July 2017)

Molecular simulation is a powerful tool for investigating microscopic behavior in various chemical systems, where the use of suitable models is critical to successfully reproduce the structural and dynamic properties of the real systems of interest. In this context, molecular dynamics simulation studies of self-assembly processes in metal-organic frameworks (MOFs), a well-known class of porous materials with interesting chemical and physical properties, are relatively challenging, where a reasonably accurate representation of metal-ligand interactions is anticipated to play an important role. In the current study, we both investigate the performance of some existing models and introduce and test new models to help explore the self-assembly in an archetypal Zn-carboxylate MOF system. To this end, the behavior of six different Zn-ion models, three solvent models, and two ligand models was examined and validated against key experimental structural parameters. To explore longer time scale ordering events during MOF self-assembly via explicit solvent simulations, it is necessary to identify a suitable combination of simplified model components representing metal ions, organic ligands, and solvent molecules. It was observed that an extended cationic dummy atom (ECDA) Zn-ion model combined with an all-atom carboxylate ligand model and a simple dipolar solvent model can reproduce characteristic experimental structures for the archetypal MOF system. The successful use of these models in extensive sets of molecular simulations, which provide key insights into the self-assembly mechanism of this archetypal MOF system occurring during the early stages of this process, has been very recently reported. Published by AIP Publishing. [<http://dx.doi.org/10.1063/1.4994700>]

I. INTRODUCTION

Self-assembly processes are ubiquitous both in the biological world and in chemical syntheses. Specifically, in the field of nanoscience, self-assembly offers the potential to develop “bottom-up” strategies for fabricating nanoscale assemblies or materials with remarkable functionalities. To this end, exploratory methods are often employed by experimentalists. An understanding of self-assembly mechanisms would greatly aid in the development of successful and efficient design strategies. A detailed understanding of self-assembly mechanisms would include characterization of various molecular level ordering processes or events and their spatial and temporal connections. However, investigations of microscopic structures and molecular mechanisms of formation by direct experimental studies are often difficult. Computer simulations afford opportunities for detailed molecular-level examination of self-assembly processes and have been used previously to reveal the underlying mechanisms in a variety of systems including proteins,^{1–5} lipids,^{6–12} biomolecules,^{13–15} gas-hydrates,^{16–18} and various nano-materials.^{19–21} Investigation of self-assembly processes of nano-structured materials through molecular simulations is an interesting albeit challenging area of research. This can be attributed to the relatively complex physical and chemical processes that underlie the formation of such structures.

Metal organic framework (MOF) materials are a class of crystalline solid-state porous (micro- to meso-porous) materials^{22–25} with many interesting structural and functional characteristics. The porous nature of MOFs distinguishes them from traditional coordination polymers. MOFs consist of metal ions, typically of transition metals,²⁶ 3p-metals²⁶ or lanthanides,²⁷ and organic ligands, usually aromatic carboxylates or phosphonates, that are arranged in two- or three-dimensional periodic network structures. In MOF structures, the metal ions (either a single ion or clusters of ions) constitute the vertices and are linked by the organic ligands. These vertices, characterized by a specific ligand topology around metal ion centers, are often referred to as “secondary building units” (SBUs) in the MOF literature for ease of structural characterization and classification of MOFs.²⁸ SBUs are typically distinguished on the basis of their overall topology and SBUs with different coordination geometries have been observed in experiments, e.g., triangular tetrahedral rectangular, square paddle-wheel, distorted rectangular, square pyramidal trigonal prismatic, octahedral, and hexagonal SBUs.^{29,30}

While various combinations of metal-ions and organic ligands in specific solvent environments have led to syntheses of a multitude of MOFs, very little is known about the underlying MOF self-assembly process. Only a few experimental studies have directly explored the formation mechanisms in MOFs.^{31–38} Self-assembly of MOFs typically involve multiple components (such as the metal ions, ligands, deprotonating

^{a)}E-mail: pkusalik@ucalgary.ca

bases, and single or mixed solvents) making detailed examinations of the underlying chemical and physical processes during MOF self-assembly inherently challenging. In this study, we investigate and compare the behavior of models appropriate for classical molecular dynamics (MD) simulations that can be used to explore the underlying physical processes associated with the self-assembly of archetypal Zn-carboxylate MOF systems.

Successful MD simulations require suitable models that can efficiently reproduce the key interactions within the system of interest. The development of appropriate models has remained a challenging problem for complex chemical systems in general. In the context of simulating MOF self-assembly, for example, simulation systems require at the least three components, i.e., metal ions, ligands, and solvents. For such systems, the use of simple yet effective models in classical simulations enable the exploration of relatively long time and large length scale events, e.g., self-assembly and crystallization processes,^{39–44} but such models require validation.

In order to reasonably reproduce experimental structures and energetics, three types of approaches have been implemented for modeling transition and alkaline earth metal ions in classical MD simulations: (1) non-bonded point charge models;^{45,46} (2) covalent bonded models;^{47,48} and (3) cationic dummy atom (CDA) models.^{49,50} It has been observed that simple non-bonded models are usually inadequate for reproducing experimental structures and energetics, particularly for metalloprotein systems containing transition metal ions.^{51,52} As an alternative approach for reproducing experimental structures and preserving the coordination geometry of the metal ions during MD simulations, bonded models, in which covalent bonds are introduced between metal-ions and ligands to fix the specific coordination structure, have been implemented. Such an approach has been widely used in biomolecular simulations of systems such as Zn-ion based metalloenzymes.^{53,54} However, a predefined metal-ligand covalent bond allows for only one specific coordination geometry around the metal ions and does not allow ligand exchanges during the simulation. Accordingly, the covalent bonded model approach is not suitable for investigating self-assembly processes, where

conversion between different geometries and ligand exchange for a metal-ion can be anticipated to be important during structural evolution.

The cationic dummy atom (CDA) model approach⁵⁰ was specifically introduced to address the limitations associated with the non-bonded point charge and the covalent bonded models. In this approach, dummy atom sites are arranged around a central atomic site to mimic the directionality of coordinate bonds, thereby helping to achieve the target metal-ligand coordination geometry during simulations. The total mass of the metal ion is distributed over the central atom and the dummy atom sites, where the central atomic site retains a majority of the mass. The dummy atom sites are covalently bonded to the central atomic site to ensure rigidity and interact with other molecules only through electrostatic interactions, whereas the central atomic site interacts through van der Waals interactions alone. The CDA model has been used successfully in bio-simulation studies, where the dummy atoms are arranged around the central atom in tetrahedral⁴⁹ and octahedral⁵⁵ geometries. Furthermore, the CDA modeling approach has also been used successfully in Langevin dynamics (LD) simulations to explore the self-assembly processes in a metal-organic discrete material⁵⁶ and MOF.⁵⁷

The archetypal Zn-carboxylate MOF system of interest here consists of Zn-ions and 1,4-benzene-dicarboxylate (BDC) ligands as primary building blocks, which can assemble into several different types of MOF structures such as MOF-2,⁵⁸ MOF-3,⁵⁹ and 1-D/3-D coordination polymers^{60,61} (see Fig. 1). Although the final product depends on the particular synthesis conditions, e.g., solvents, temperatures, and bases used for deprotonation of the ligands, experiments have revealed the formation of different metastable products during synthesis of a specific MOF, such as MOF-2 or analogous MOF structures.⁶² Among the different types of MOFs or coordination polymers that can form from a Zn-carboxylate system, the MOF-2 structure serves as a prototype for a class of MOFs incorporating several types of metal ions and ligands⁶³ to form SBUs with a paddle-wheel cluster (PWC) topology. MOF-2 also represents one of the simplest MOF structures that can be assembled in a variety of aprotic polar solvent media [e.g.,

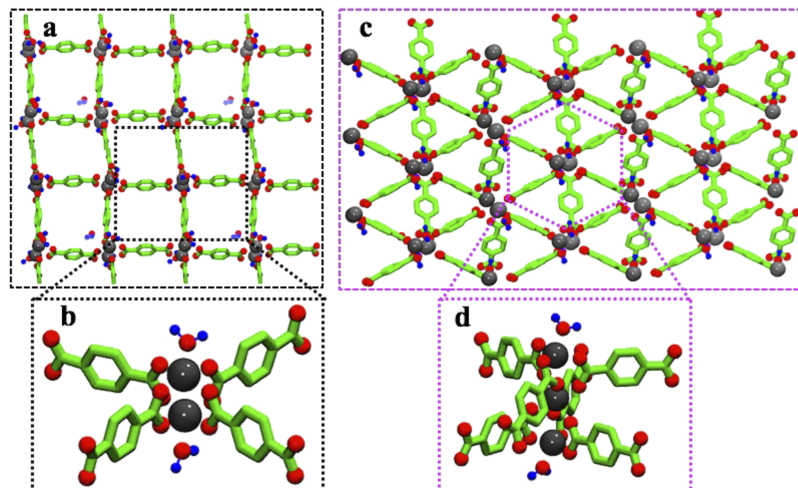


FIG. 1. Two of the possible MOF structures and the corresponding SBUs that can form in Zn-carboxylate systems. (a) Periodic MOF-2 structure;⁵⁴ (b) paddle-wheel cluster that constitutes the vertices of the MOF-2 structure; (c) periodic MOF-3 structure;⁵⁵ (d) trimeric Zn-ion cluster that comprises the vertices in the MOF-3 structure. The Zn-ions and BDC ligands are gray and green, respectively. The two water molecules at the axial coordination-sites of the Zn-ions are shown in blue and red CPK representation.

N,N'-dimethylformamide (DMF),⁶⁴ *N,N'*-diethylformamide (DEF),⁶⁴ dimethyl sulfoxide (DMSO)⁶⁵] and over a range of temperatures, and the formation of a MOF-2 like structure does not involve complex chemical reactions, such as covalent bond rearrangement. In this study, an experimental MOF-2 crystal structure was selected for model validation, where successful potential models are also expected to be valid for other similar MOFs, such as a MOF-3 structure. Importantly, models identified as being suitable are anticipated to demonstrate the assembly of structural motifs resembling PWCs (i.e., the SBUs in MOF-2) during simulations, as well as structural motifs resembling other types of SBUs, e.g., monomeric Zn-ions and trimeric Zn-ion clusters.

In the current study, we have examined various metal-ion and solvent models to investigate the model dependence in the structural behavior of an archetypal Zn-carboxylate MOF system during self-assembly. Non-bonded point charge and CDA models representing metal ions are examined and compared. Additionally, an extended CDA (ECDA) model is designed and validated for simulations of Zn-carboxylate systems. The behavior of dipolar solvent models is compared to that of both a continuum solvent and an explicit *N,N'*-dimethylformamide (DMF) solvent model, DMF being a typical solvent used in experiments. Free energy calculations are performed to help assess the validity of the various models. The relative free energies obtained through these calculations are used to help explain the observation of the formation of specific structural motifs (or SBUs) reported in experiments^{58–62} and in our previous simulations.⁶⁶ This study demonstrates that the ECDA Zn-ion model, in combination with a simple dipolar solvent model, can be used effectively to explore the longer time scales associated with the complex ordering processes in the archetypal Zn-carboxylate MOF system of interest.

II. MODELS AND METHODS

A. Primary building blocks

The formation of an archetypal Zn-carboxylate MOF requires a minimum of three components, i.e., Zn-ions, BDC ligands, and solvents. The current study examines rigid models corresponding to these three principal components. Acetate ions were also introduced as monotopic carboxylate ligands into the simulation systems. This was primarily because the acetate ions can serve as capping ligands to allow assembly of PWC motifs and discrete MOF-2-like square arrangements. We also note that the smaller acetate ions have a somewhat shorter residence time around Zn-ions than BDC ligands, thereby facilitating a faster rate of structural rearrangement. The influence of three different solvent models, i.e., dipolar, DMF, and continuum solvents, was investigated. For explicit solvent simulations, the typical test system consisted of eight Zn-ions, four BDC ligands, four acetate ions, and appropriate numbers of dipolar/DMF solvents, i.e., to provide solutions with Zn-ion concentrations corresponding roughly to those used in experiments. Similarly, the typical continuum solvent test system consisted of eight Zn-ions, four BDC ligands, and four acetate ions. These specific test systems (with respect to the number of metal ions and ligands) allowed the exploration

of behavior of systems that can assemble into four PWCs or a single MOF-2-like square arrangement. System size dependence and its influences on self-assembly processes have been discussed in our previous work.⁶⁶ In general, it was found that smaller systems tend to favor fewer large Zn-ion cluster sizes (e.g., 5 Zn-ion or 4 Zn-ion cluster) being formed during simulations, on account of the limited number of Zn-ions available in the system, without significantly affecting the basic self-assembly process.

B. Non-bonded, CDA, and ECDA Zn-ion models

To probe the behavior of the Zn-ion models important for self-assembly, three types of Zn-ion models were examined, a non-bonded point charge, a CDA, and an ECDA model (see Fig. 2). Since charge transfer, from coordination ligands to metal-ions, is known to play an important role in the coordinating behavior of transition metal-ions,⁶⁷ its effect on structural and thermodynamics behavior of an archetypal Zn-carboxylate system was investigated in the current study. Within a simplified (i.e., effective) potential, the charge transfer effect can be implicitly incorporated by reducing the net charge of the model Zn-ions.⁶⁸ Accordingly, a reduced charge value of +1.4 was assigned to the Zn-ion models, where we note that similar reduced charge values for Zn-ion models have been used in other simulation studies.⁶⁹ The two Zn-ion models carrying net charge values of +1.4 and +2 will be referred to as models (I) and (II), respectively. For example, the non-bonded models carrying charges +1.4 and +2 are termed as non-bonded(I) and non-bonded(II) models, respectively.

The CDA model implemented in this study (which is a modified version of the original CDA model⁵⁰) has a square planar geometry, where the dummy atom sites are 0.9 Å from the central atomic site. Each of the four dummy atoms possesses a charge value of +0.35 and +0.5 for the CDA(I) and CDA(II) models, respectively. The short-range force-field parameters [i.e., Lennard-Jones (LJ) parameters] of the original Zn-ion CDA model were found to be inappropriate for the current study (i.e., unable to reproduce experimental MOF structure), and consequently values from another previous simulation study⁴⁵ were adopted. The extended CDA, or ECDA,

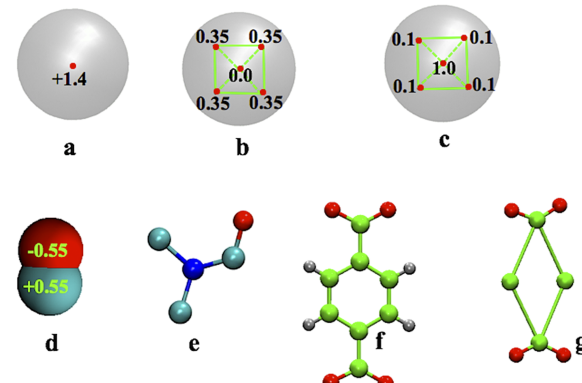


FIG. 2. Three different Zn-ion models, two explicit solvent models, and 1,4-benzene-di-carboxylate ligand models used in this study. (a) Non-bonded(I) Zn-ion model; (b) CDA(I) Zn-ion model; (c) ECDA(I) Zn-ion model; (d) solvent 0.55 dipolar solvent model; (e) united-atom DMF solvent model; (f) all-atom 1,4-BDC ligand model; and (g) coarse-grained 1,4-BDC ligand model.

models (I and II) are similar to the CDA models in that a square planar geometry is imposed on the four dummy atom sites attached to the central atom site. However, the charge distribution for the ECDA model has been adjusted, where each of the dummy atoms carries a partial charge of $+\delta$, while the central atom possesses a charge of $(q - 4\delta)$, thereby yielding a net charge of $+q$ ($q = +2$ or $+1.4$) on the ECDA Zn-ion model. A partial charge value of $+0.1$ for the dummy atomic sites was found to work well.

C. Ligand models

Standard OPLS (Optimized Potentials for Liquid Simulations) force-field parameters⁷⁰ were used for the LJ interactions for both monotopic and ditopic carboxylate ligands, i.e., acetate and BDC ligands (see Table S1 in the [supplementary material](#)). Both all-atom and united atom models using OPLS force-field parameters⁷⁰ for the acetate ion were explored and were found to have no significant impact on the observed behavior. The behavior of a coarse-grained BDC ligand model is briefly considered in the [supplementary material](#). The charge distributions on the carboxylate groups of the ligands were modified according to the net charge of the Zn-ion model in the systems. Specifically, the acetate and BDC ligands carry a net charge of -1 and -2 , respectively, for the systems consisting of type II Zn-ion models (with a net charge of $+2$), and the acetate and BDC ligands carry a net charge of -0.7 and -1.4 , respectively, for the systems incorporating type I Zn-ion models (with a net charge of $+1.4$).

D. Solvent models

As mentioned earlier, three different solvent models were examined in the current study. A simple dipolar solvent model (see Fig. 2) was designed for computational expediency in explicit solvent MD simulations. Dipolar solvent molecules consist of two atomic sites carrying equal magnitude and opposite sign charges separated by a distance of 1 \AA ; LJ interaction parameters of an oxygen atom from the OPLS force field⁷⁰ (to mimic short-range interactions of a polar DMF-like solvent) were employed for both atoms of the molecule. By varying the magnitude of the partial charges on both the atomic sites, solvent models with different polarities were generated. For example, a solv-0.2 model carries charges of ± 0.2 and has a dielectric constant of ~ 4 at 300 K ; a solv-0.6 model possesses charges of ± 0.6 and has a dielectric constant of ~ 107 at 300 K . Table S2 in the [supplementary material](#) lists the dipole moments and dielectric constants at 300 K for the different dipolar solvent models. We point out that these epsilon values do not fully characterize solvent behavior, particularly at smaller separations where other factors will impact the short-range interactions. Thus, it was also important for the solvent model to mimic the structural behavior of a more realistic solvent such as DMF.

A united atom model for the DMF molecule (see Fig. 2), using OPLS force-field parameters,⁷⁰ was employed in the explicit DMF solvent MD simulations. The structural characteristics and dynamics of explicit DMF solvent systems were compared to those of explicit dipolar solvent and continuum solvent systems to assess if a simplified solvent model could be reasonably employed to enable exploration of longer time

scale and larger length scale ordering events. In addition to the DMF solvent model, an all-atom toluene model (using OPLS force-field parameters) was also used in explicit solvent simulations for free energy calculations. The non-bonded force field parameters for the various solvent models are provided in Table S1 of the [supplementary material](#).

In the continuum solvent simulations, purely repulsive Weeks-Chandler-Andersen (WCA) potentials⁷¹ were used to model short ranged interactions between all types of atoms except those between metal ions. Utilization of WCA potentials helps preventing the collapse of the otherwise open structures formed during simulations; a similar approach was used in previous continuum solvent simulation studies of MOF formation.^{56,57} The continuum solvent simulations were performed via Langevin dynamics (LD), where solvent screening of the electrostatic interactions was achieved by varying the dielectric constant (ϵ) of the continuum solvent medium. Similar to previous work,⁵² three ϵ values were considered, $\epsilon = 2$, 2.5 , and 3 , to explore their effects on self-assembly processes.

E. Model validation procedure

The performance of the six Zn-ion models was examined by comparing their abilities to reproduce key structural features of an experimental MOF-2-like structure. Specifically, we aimed to reproduce the experimental Zn–Zn and Zn–O (carboxylate oxygen) distances in the PWCs that constitute the vertices of a MOF-2-like structure. Accordingly, a periodic unit cell of an experimental MOF-2-like crystal structure was constructed which consists of eight Zn-ions, eight BDC ligands, and eight water molecules in a rectangular simulation box. Simulations of this periodic structure were performed in explicit dipolar (sol-0.3) solvent, explicit DMF solvent, and continuum solvent ($\epsilon = 1$) media. The LD simulations with $\epsilon = 1$ mimic the desolvated conditions in which experimental crystal structures are determined and thus should be the most appropriate for comparison with an experimental MOF-2 structure.⁵⁸ The simulations were performed for the CDA(I), ECDA(I), and non-bonded(I) Zn-ion models, and the behavior of these systems was compared to those incorporating CDA(II), ECDA(II), and non-bonded(II) Zn-ion models. For all types of simulation systems, initial energy minimizations were performed using a steepest descent algorithm, which was followed by 100 ps equilibration at a temperature of 300 K and pressure of 1 bar . Production simulations of 1 ns (at $T = 300 \text{ K}$, $P = 1 \text{ bar}$) for each of the Zn-ion models were performed, where the trajectories were sampled every 1 ps to calculate the Zn–Zn and Zn–O radial distribution functions.

In addition, various sets of MD simulations (typically including ten independent trajectories for each set) were performed to investigate the differences in structural and self-assembly behavior of the systems in which different types of Zn-ion, ligand, and solvent models were employed. These trajectories were typically at least 100 ns in length.

F. Simulation methods

All simulations were performed using the GROMACS software package.⁷² For the MD simulations of explicit solvent systems, the leapfrog algorithm was used to integrate

the equations of motion with a time step of 2 fs. A 12-Å cutoff distance was applied for the Lennard-Jones interactions (long-range corrections were applied), and particle-mesh Ewald (PME) summations⁷³ were used to evaluate the long-range electrostatic interactions. A Berendsen thermostat⁷⁴ with a coupling constant of 0.1 ps was used to maintain the temperature during simulations. The LINCS algorithm⁷⁵ was utilized for bond constraints, and periodic boundary conditions were imposed for all simulations. For the continuum solvent systems, LD simulations were performed with the leapfrog stochastic dynamics integrator with a time step of 2 fs, and a stochastic thermostat with a time constant $\tau_t = 0.1$ ps was used to maintain the temperature. The default friction coefficient in GROMACS (which is given by mass/ τ_t for each particle) was employed for the LD simulations.

G. Calculation of relative free energies ($\Delta\Delta G$)

The archetypal Zn-carboxylate system under investigation here can produce a variety of cluster topologies that constitute the vertices/SBUs of various polymeric/MOF structures as evidenced by the multitude of Zn-carboxylate crystal structures reported by experimental studies.⁶² For example, Zn-ions and BDC ligands have been observed, both in experimental studies and in our previous simulation work employing the ECDA(I) Zn-ion model,⁶⁶ to form a variety of structural motifs (see Fig. 3) such as PWC (or PWC-4), PWC-3 (two Zn-ions bridged by three carboxylate groups), trimeric Zn-ion clusters (three Zn-ions bridged by six carboxylate groups), and monomeric Zn-ion complexes (one Zn-ion coordinated to two carboxylate groups). To explore thermodynamic factors that might affect

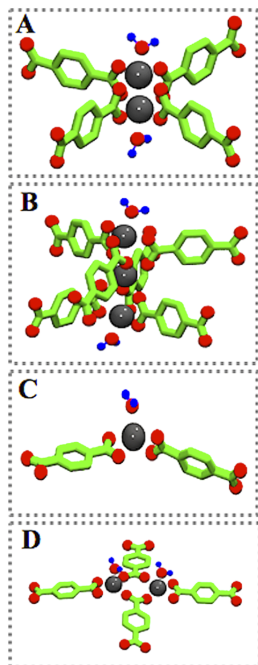


FIG. 3. The four selected structural motifs (or SBUs in MOF structures) examined in relative free energy calculations. (a) PWC-4 motif or the SBU of a MOF-2 structure;⁵⁴ (b) trimeric Zn-ion cluster or the SBU of a MOF-3 structure;⁵⁵ (c) monomeric Zn-ion complex that constitutes the vertices of a 1-D coordination polymer;⁵⁶ and (d) dimeric Zn-ion cluster that constitutes the vertices of a 2-D MOF structure.⁵⁷ Ions and ligands appear as in Fig. 1.

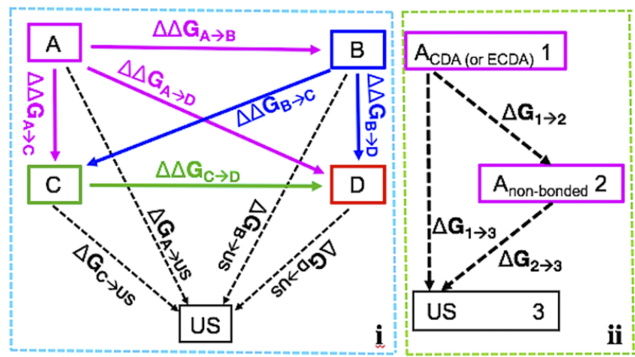


FIG. 4. Panel (i) presents a schematic diagram for calculation of free energy differences per Zn-ion ($\Delta\Delta G$) between four selected Zn-ligand structural motifs, A–D (see Fig. 3). The end state, US, in each of the primary free energy calculations represents an ideal unstructured state, where the electrostatic interactions between the Zn-ions and carboxylate ligands are set to zero. Panel (ii) shows a representative scheme for validation of $\Delta\Delta G$ calculations in systems employing either the CDA(I) or ECDA(I) Zn-ion model, where $\Delta G_{1 \rightarrow 3}$ must be equivalent to $\Delta G_{1 \rightarrow 2} + \Delta G_{2 \rightarrow 3}$ [1 → 2 represents conversion of CDA(I) or ECDA(I) Zn-ions to a non-bonded(I) model; 2 → 3 represents conversion of a non-bonded(I) Zn-ion to the US state].

formation of these structural motifs, calculations of relative free energies were carried out on four selected discrete Zn-ion BDC-ligand clusters or structural motifs, i.e., (a)–(d), in Fig. 3. Because the four chosen motifs consist of different numbers of Zn-ions and BDC ligands, the free energy of formation per Zn-ion (ΔG) from a common reference state was estimated for each motif, where the thermodynamic integration method⁷⁶ was employed. An ideal unstructured state, US, in which the Coulombic interactions between Zn-ions and carboxylate ligands are turned off, was defined as the common reference state. Accordingly, the free energy of dissociation per Zn-ion, i.e., $\Delta G_{A \rightarrow US}$, $\Delta G_{B \rightarrow US}$, $\Delta G_{C \rightarrow US}$, and $\Delta G_{D \rightarrow US}$, was calculated for each of the four motifs. The free energies of formation per Zn-ion for the four motifs were then compared by determining the relative free energy differences ($\Delta\Delta G$), e.g., $\Delta\Delta G_{A \rightarrow B}$ is the relative free energy difference between the discrete states A and B. As free energy is a state function, the transformation from motif A to motif B can be made via a real or fictitious thermodynamic path. These free energy calculations were performed in two different solvent media, a non-polar toluene and a polar DMF solvent, for all six Zn-ion models. The free energy differences (i.e., $\Delta\Delta G$ values) were used to characterize schematic thermodynamic transitions connecting the four selected clusters (see Fig. 4).

III. RESULTS AND DISCUSSION

A. Zn-ion model validation

The strength of electrostatic interactions between Zn-ions and carboxylate oxygens is greatest for systems with the CDA Zn-ion model and smallest for systems using the non-bonded Zn-ion model. The increased magnitude of electrostatic interaction for systems with the CDA Zn-ion model arises due to the reduced distance between the positive charge sites (i.e., the dummy atoms) and the carboxylate oxygens compared to the distance between the point charge at the center of the Zn-ion and carboxylate oxygens as in the non-bonded Zn-ion model.

The ECDA Zn-ion model exhibits characteristics intermediate between those of the non-bonded and CDA models as both the center site and dummy atom sites carry partial charges. These basic features of the Zn-ion models will be important in the discussions below.

Figure 5 shows snapshots of a periodic MOF-2-like square arrangement from continuum solvent ($\epsilon = 1$) LD simulations employing the non-bonded(I), CDA(I), and ECDA(I) Zn-ion models and compares the Zn–Zn and Zn–O (carboxylate oxygen) radial distribution functions (rdf's) for these systems. Visualization of the trajectory for the system using the ECDA(I) model revealed that the square pyramidal coordination geometry of each Zn-ion (i.e., Zn-ion coordinated to four carboxylate oxygens and one water oxygen) and the periodic MOF-2-like square arrangement were maintained during simulation [see Fig. 5(c)]. While the CDA(I) model was also able to maintain the periodic MOF-2-like square arrangement, it was not able to preserve the square pyramidal coordination geometries of the Zn-ions [see Fig. 5(b)]. Specifically, some of the water molecules at the axial coordination sites of the Zn-ions were displaced during the simulation. The non-bonded(I) Zn-ion model was unable to preserve the square pyramidal coordination geometry [see Fig. 5(a)], rather preferring a distorted octahedral coordination geometry for the Zn-ions. This coordination preference in turn distorts the PWCs in the periodic MOF-2-like structure.

In explicit dipolar and DMF solvent simulations, the CDA(I), ECDA(I), and non-bonded(I) Zn-ion models exhibit structural characteristics similar to those observed in continuum solvent simulation (see Figs. S1 and S2 in the [supplementary material](#)). However, the effect of screening by polar DMF solvent molecules on the interactions between carboxylate oxygens and Zn-ions is apparent in all three systems, most dramatically observed through wider peaks in the Zn–Zn rdf for the system with the non-bonded(I) Zn-ion model. A similar effect was also observed in explicit dipolar solvent simulations for systems with the non-bonded(I) Zn-ion model.

Figure 6 compares Zn–Zn and Zn–O rdf's and shows snapshots of the periodic MOF-2-like square arrangement from continuum solvent simulations employing the Zn-ion models carrying net charge values of +1.4 and +2. Both the CDA(II)

and ECDA(II) models exhibit characteristics similar to those of the CDA(I) and ECDA(I) models, respectively, whereas the non-bonded(II) model resulted in a distorted periodic structure with little resemblance to the MOF-2 structure. In this new structure [see Fig. 5(e)], the Zn-ion dimers are bridged by two BDC ligands and each Zn-ion is coordinated to another BDC ligand.

Experimental MOF-2 crystal structures (desolvated) yield a Zn–Zn distance of $\sim 2.94 \text{ \AA}$ and a Zn–O (carboxylate oxygen) distance of $\sim 2.01\text{--}2.07 \text{ \AA}$ in the PWCs.⁶³ A comparison of the first peaks in the Zn–Zn rdf's for model(I) Zn-ions in continuum solvent gives Zn–Zn distances of $\sim 2.57 \text{ \AA}$, $\sim 2.92 \text{ \AA}$, and $\sim 3.30 \text{ \AA}$ [see Fig. 5(d)] for the CDA(I), ECDA(I), and non-bonded(I) models, respectively. Similarly, the first peaks in Zn–O rdf's yield Zn–O distances of $\sim 1.95 \text{ \AA}$, $\sim 2.02 \text{ \AA}$, and $\sim 2.06 \text{ \AA}$ [see Fig. 5(e)] for the CDA(I), ECDA(I), and non-bonded(I) models, respectively. Although both the ECDA(I) and non-bonded(I) Zn-ion models were able to reproduce the experimental Zn–O distance, the CDA(I) model apparently prefers a slightly shorter Zn–O distance. While these Zn–O distances are within an acceptable range for all three Zn-ion (I) models, only the Zn–Zn distance obtained from the ECDA(I) model system is in good agreement with the experimental MOF-2 structure.

In explicit solvent systems (see Figs. S1 and S2 in the [supplementary material](#)), the first peak in the Zn–Zn rdf is generally wider compared to that in continuum solvent simulations, where this effect is most pronounced for the non-bonded(I) Zn-ion model. This is indicative of the distorted coordination geometry of the Zn-ions in the periodic structure of the system using the non-bonded(I) Zn-ion model. Furthermore, we also observed that the polar DMF solvent has a more pronounced effect on the Zn–Zn distance compared to the less polar sol-0.3 dipolar solvent.

A net charge value of +2 for the Zn-ions in the non-bonded(II), CDA(II) and ECDA(II) models further strengthens the attractive interactions between Zn-ions and carboxylate oxygens leading to shorter Zn–O distances for all three Zn-ion models [see Fig. 6(b)]. At the same time, the larger Zn-ion charge leads to a stronger repulsion between the two Zn-ions in a PWC. Therefore, Zn–Zn distances tend to be relatively longer for model (II) systems in comparison to those in systems

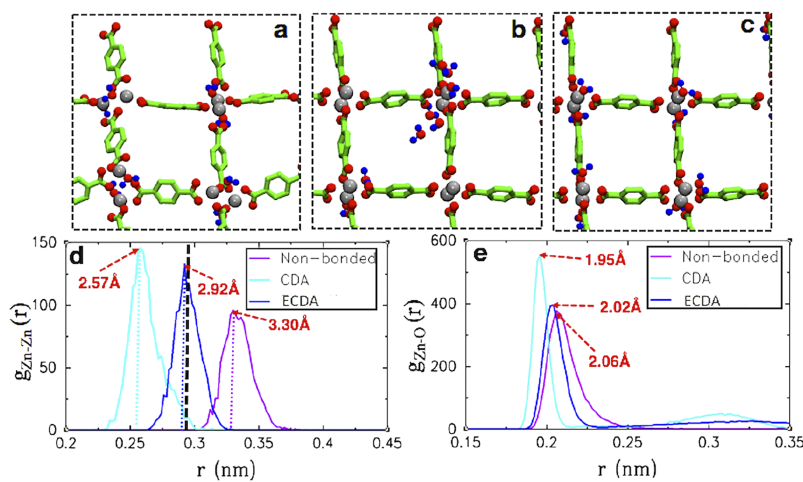


FIG. 5. Snapshots of a MOF-2 unit cell in a periodic arrangement as seen at the end of Langevin dynamics (LD) simulations ($\epsilon = 1$) performed at 300 K, for systems containing (a) non-bonded(I), (b) CDA(I), and (c) ECDA(I) Zn-ion models. The panels (d) and (e) show Zn–Zn and Zn–O radial distribution functions (rdf's), respectively, for the periodic MOF-2 structure, where the purple, cyan, and blue curves correspond to systems employing the non-bonded(I), CDA(I), and ECDA(I) Zn-ion models, respectively. Ions and ligands appear as in Fig. 1. In panel (d), the black dashed line represents the position of the 1st peak in the experimental Zn–Zn rdf for a MOF-2 structure.⁵⁴

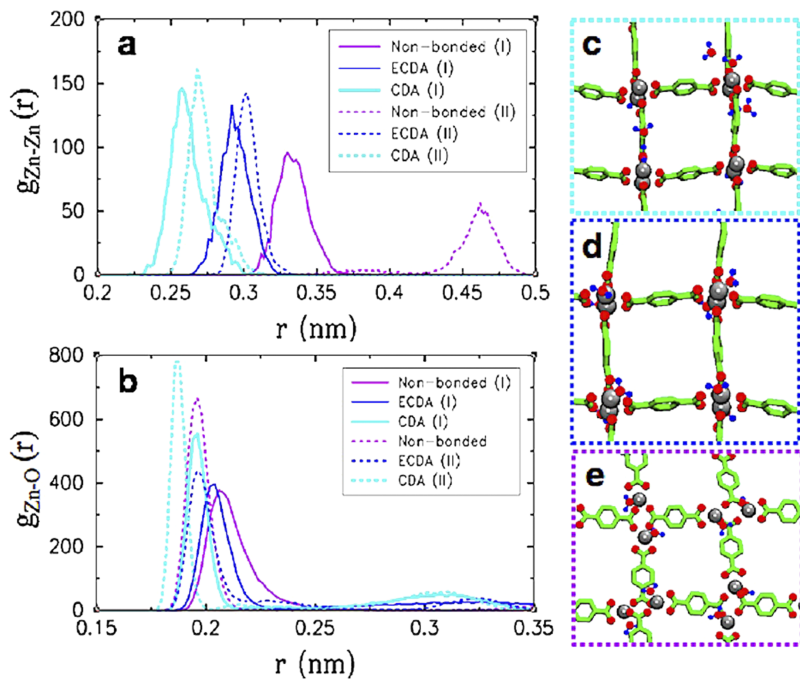


FIG. 6. Structure of a MOF-2-like square arrangement as seen at the end of LD simulations ($\varepsilon = 1$) at 300 K. Panels (a) and (b) show a comparison of Zn-Zn and Zn-O rdf's, respectively, between simulation systems employing the non-bonded(I), CDA(I), ECDA(I), non-bonded(II), CDA(II), and ECDA(II) Zn-ion models. Panels (c)–(e) show snapshots of the systems employing CDA(II), ECDA(II), and non-bonded(II) Zn-ion models, respectively, as seen at the end of the LD simulations.

employing model (I) Zn-ions. The effect of a stronger repulsion between the Zn-ions is most pronounced in the system with the non-bonded(II) model [see Fig. 6(a)]. Specifically, the Zn-Zn separation increases from 3.30 Å for the non-bonded(I) model to ~4.63 Å for the non-bonded(II) model. Our comparison of snapshots of these two systems had identified a distortion of the structure in the latter (namely, that the 3-D PWC arrangement is modified into a 2-D planar arrangement).

Overall, our results (both visualization and comparison of rdf's) reveal that the ECDA(I) Zn-ion model is superior to the other models examined and performs well in reproducing the experimental MOF-2 structure. The performance of these models in predicting the relative thermodynamic stabilities of several key structures will now be investigated.

B. Relative free energy calculation

In the simulations supporting our relative free energy calculations, transformations of the original structures were sometimes observed to occur for specific combinations of Zn-ion and solvent models. For example, the structural motifs A and D sometimes transformed into a fifth type of structure, labeled as motif E (see Fig. 7). Similarly, structural motif B appeared to transform into a sixth type of structure, labeled as motif F, in toluene solvent systems employing the CDA(I) model (see Fig. 7). The structural motif E has a PWC-3 like topology, where two Zn-ions are bridged by three BDC ligands with one Zn-ion being coordinated to the fourth BDC ligand. Such an arrangement around the Zn-ions generates a combination of tetrahedral/pseudo-octahedral or tetrahedral/trigonal-bi-pyramidal coordination geometries for the two Zn-ions in

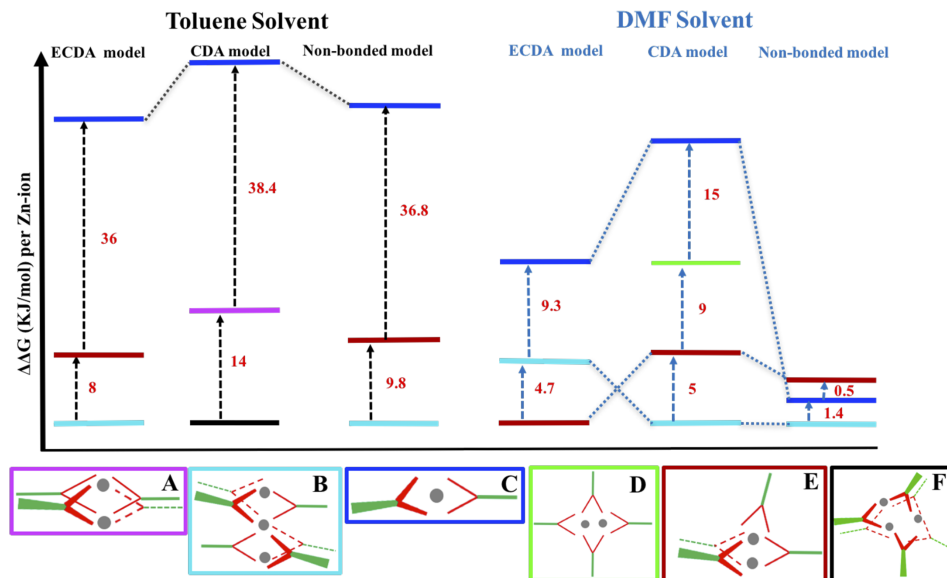


FIG. 7. Zn-ion model dependence of the difference in free energy per Zn-ion ($\Delta\Delta G$) between the structural motifs (a)–(f) solvated in toluene and DMF solvents at a temperature of 300 K. In this schematic diagram, the magenta, cyan, blue, green, red, and black lines correspond to the relative free energies of the structural motifs (a)–(f), respectively. Schematic representations for each of these structural motifs are also given, where we note that the structural motif (e) is seen to arise from simulations starting from motifs (a) and (d) in specific combinations of Zn-ion and solvent models (see discussion in text). Structural motif (f) is seen to arise from simulations starting from motif (b) in toluene solvent systems employing the CDA Zn-ion model. The dotted lines, which have been added to aid comparison, connect values for the same structures.

the structural motif E. Structural conversions between motif A and motif E (or structural variants of motif E) were observed both in explicit toluene solvent systems with the ECDA(I) and non-bonded(I) Zn-ion models and in explicit DMF solvent simulations with all three Zn-ion (I) models. Similarly, structural conversion between motif D and motif E was noted both in DMF and toluene solvent systems with the non-bonded(I) and ECDA(I) Zn-ion models and in the explicit toluene solvent simulation with the CDA(I) Zn-ion model. These structural transformations indicate that a discrete PWC-4 motif is apparently stable only in relatively non-polar solvents employing the CDA(I) Zn-ion model. In structural motif F, the three Zn-ions with six bridging carboxylates and two water molecules are arranged into a trigonal motif, where each Zn-ion attains a square planar geometry. The transformation from motif B to F in toluene solvent can be understood on the basis of the strong preference of the CDA(I) model for a square planar geometry rather than the tetrahedral geometries of the two terminal Zn-ions in motif B. Although structural conversion between motifs B and F was not observed for the CDA(I) model in explicit DMF solvent, the coordination structure of the two Zn-ions in motif B changes from tetrahedral to square planar (see Fig. 7).

The calculations of relative free energies per Zn-ion (see Fig. 7) reveal that motifs B, B, and F represent structural entities with the lowest free energies in an explicit toluene solvent system employing the non-bonded(I), ECDA(I), and CDA(I) Zn-ion models, respectively. Explicit DMF solvent systems with the non-bonded(I), ECDA(I), and CDA(I) Zn-ion models feature motifs B, E, and B, respectively, as the lowest free energy structures (see Fig. 7). In explicit DMF solvent systems, the order with respect to decreasing relative free energies is C > B > E with the ECDA(I) model, C > D > E > B with the CDA(I) model, and E > C > B with the non-bonded(I) model (although the differences are small). In explicit toluene solvent systems, the order with respect to decreasing relative free energies is C > E > B with the ECDA(I) model, C > A > F with the CDA(I) model, and C > E > B with the non-bonded(I) model. The structural motif C, i.e., the monomeric Zn-complex, has the highest relative free energy in non-polar solvent systems with all three Zn-ion (I) models and in polar solvent systems with the ECDA(I) and CDA(I) Zn-ion (I) models. This observation can be correlated to the gas-phase density functional theory (DFT) calculation of Bureekaew *et al.*,⁷⁷ which reported that the formation of a dimeric Zn-ion based PWC-4 motif from two monomers is energetically downhill. Therefore, monomeric Zn-ion complexes (e.g., motif C) can be anticipated to form primarily as kinetic products prior to formation of dimeric Zn clusters (either motif A or motif E) during self-assembly processes in Zn-carboxylate systems. In general, the relative free energy calculations revealed that Zn-ions have a relatively higher probability of forming both trimeric and dimeric Zn-ion clusters, while monomeric Zn-ion (and ligand) clusters are less likely to assemble during simulations. These results correlate with the early stage self-assembly mechanism in this archetypal Zn-carboxylate MOF system employing the ECDA Zn-ion model.⁶⁶ For example, monomeric Zn-ions coordinated by one or two carboxylate ligands and forming chain like structures/fragments were observed to assemble

first during the self-assembly process (i.e., as kinetic products). Later, the monomeric Zn-ligand complexes transformed into dimeric (structural motif E) and trimeric (structural motif B) Zn-ligand complexes. Moreover, there is general consensus between simulations and experimental observations with respect to Zn-ions tending to prefer dimeric and trimeric Zn-carboxylate clusters when combined with rigid carboxylate ligands.⁷⁸

In the absence of experimental free energy estimations, qualitative free energy trends may be predicted from structural trends. For example, an *in situ* crystallography experiment, focused on MOF-2 synthesis at room temperature,⁶² showed evidence of formation of a MOF-3-like structure prior to structural conversion to MOF-2. Accordingly, a MOF-2-like structure (consisting of PWC-4, or structural motif A, as SBUs) can be anticipated to have lower free energy than a MOF-3-like structure (consisting of trimeric Zn-ion clusters, or structural motif B, as SBUs). Additionally, experimental studies have revealed that PWC-3 motifs are more frequently observed compared to the PWC-4 motifs⁶³ as vertices of Zn-ion based coordination polymers or discrete coordination complexes. During the free energy calculations, PWC-4 motifs were observed to transform into PWC-3 motifs in both polar and non-polar solvent systems with ECDA(I) or non-bonded(I) Zn-ion models and in a polar DMF solvent system with the CDA(I) model. The conversion between a PWC-4 and a PWC-3 motif can be explained on the basis of an entropy effect, as a PWC-4 motif is more ordered (i.e., appears more rigid) compared to a PWC-3 motif. Hence, a discrete PWC-3 motif is expected to be favored in the absence of stronger enthalpic compensations. For systems with the CDA(I) Zn-ion model, the increased electrostatic interaction between the Zn-ions and carboxylate oxygens possibly outweighs the entropic penalty, thereby stabilizing the PWC-4 motif relative to the PWC-3 motif.

Based on the estimated free energy trends from Fig. 7, the apparent structural preferences exhibited by the three Zn-ion (I) models can be correlated with structural preferences of alkaline earth and transition metal-ions. For example, Mg²⁺ is a spherical ion and does not have specific coordination preferences. In this context, the behavior of the non-bonded model is more consistent with the behavior of a typical Mg-ion, whereas the CDA model imparts a stronger coordination behavior to the metal-ion, and is thus more suitable to mimic a transition metal-like ion. On the other hand, the ECDA model is a compromise between the non-bonded model and CDA model. Therefore, the ECDA model performs better to represent a Zn-ion with relatively flexible coordination geometries (but not as flexible as alkaline earth metal-ions like Mg-ion).

C. Characterization of solvent relaxation

Given the strong electrostatic interactions between Zn-ions and carboxylate ligands that drive the self-assembly processes, a dipolar solvent model with appropriate polarity is necessary to provide the electrostatic screening necessary for facilitation of structural rearrangements over reasonable time scales. To this end, multiple sets of simulations were performed for the test systems (described in Sec. II) with different dipolar

solvents, i.e., sol-0.2, sol-0.3, sol-0.4, sol-0.5, sol-0.55, sol-0.6, where the term sol- x refers to a specific dipolar solvent model with partial charges $\pm x$ on the two atomic sites (see Table S2 in the [supplementary material](#) for the dielectric constants of various dipolar solvents). These test systems used the ECDA(I) model to represent Zn-ions.

To help examine how different solvents influence the dynamics of these systems, residence time correlation functions (RTCFs) of solvents around Zn-ions were determined. The RTCF is given by⁷⁹

$$P_{ij}(\tau) = \int \delta(N_{ij}(t) - N_{ij}(t + \tau)) dt, \quad (1)$$

where $\delta(N_{ij}(t) - N_{ij}(t + \tau)) = 1$ when $N_{ij}(t) = N_{ij}(t + \tau) \neq 0$ and $\delta(N_{ij}(t) - N_{ij}(t + \tau)) = 0$ when either $N_{ij}(t) \neq N_{ij}(t + \tau)$ or $N_{ij}(t) = N_{ij}(t + \tau) = 0$. The value of $N_{ij}(t)$ is equal to 1 if the solvent molecule j at time t is found within the solvation sphere (defined by a cutoff radius) of the Zn-ion i , and zero otherwise. The cutoff radius of 2.5 Å was determined from the Zn-solvent radial distribution function for this solution system. The average value of the integral in Eq. (1) was evaluated by summing and averaging it over all the Zn-ions and solvent molecules in the system. Table I provides Zn-solvent relaxation times extracted from bi-exponential fits to the Zn-solvent residence time correlation functions for different dipolar solvents at 300 K and 450 K, where the RTCFs were averaged over three trajectories for each solvent type (Fig. S3 in the [supplementary material](#) shows example RTCFs for simulations performed at 300 K). In these bi-exponential fits, $y = a_0 + a_1 e^{-t/\tau_1} + a_3 e^{-t/\tau_2}$, τ_1 and τ_2 represent the short and long relaxation times, and a_1 and a_3 are their corresponding weights, respectively. A comparison of the Zn-solvent relaxation times at the two temperatures studied, 300 and 450 K, shows shorter solvent residence times at higher temperature, as expected, for all types of dipolar solvents.

Similar to the calculation of Zn-solvent RTCFs, Eq. (1) was used to calculate RTCFs of carboxylate oxygens (i.e., where j is now a carboxylate oxygen) around Zn-ions in different solvent systems. However, the relaxation times of the ligands were typically too long to be reasonably quantified and compared across different dipolar solvents; for example, the Zn-ligand RTCF in sol-0.3 and sol-0.4 dipolar solvents was observed to essentially show no decay over 30 ns of simulation.

A shorter residence time of solvent molecules is indirectly linked with a longer residence time of carboxylate ligands

TABLE I. Zn-solvent residence time as obtained from bi-exponential fits to the residence time correlation functions for different dipolar solvent systems at 300 K and 450 K.

Dipolar Solvent	Residence time at 300 K		Residence time at 450 K	
	τ_1 (ps)	τ_2 (ps)	τ_1 (ps)	τ_2 (ps)
sol-0.3	37	1.7×10^2	3.0	53
sol-0.4	83	3.8×10^2	33	86
sol-0.5	4.7×10^2	2.8×10^3	44	1.4×10^2
sol-0.6	7.1×10^2	8.8×10^3	79	3.2×10^2

around Zn-ions, as observed in sol-0.3 and sol-0.4 solvent systems, for example. A shorter residence time of ligands around the Zn-ions would imply a faster rate of structural rearrangements during self-assembly processes, for example, as observed in sol-0.6 solvent systems. From the qualitative and quantitative comparison of Zn-ligand and Zn-solvent RTCFs, it appears that systems with relatively high polarity solvents (e.g., sol-0.6, sol-0.55, and sol-0.5) at high temperature (e.g., 450 K) can be suitably used to explore self-assembly processes within a reasonable computational time (e.g., 1 μs). Nevertheless, a suitable solvent medium should also be able to produce key structures or motifs (e.g., PWC-3 motifs) expected for this archetypal Zn-carboxylate system, while aiding in a reasonably fast structural rearrangement during simulations.

Figure 8 shows Zn-Zn rdfs, each averaged over ten trajectories, in explicit DMF solvent systems within four different time windows (0–10 ns, 10–50 ns, 50–250 ns, and 500–1000 ns). The inset figure shows the same in explicit sol-0.3 dipolar solvent systems within two time windows, i.e., 0–10 ns and 10–50 ns. A comparison of the time evolution of the rdfs between the DMF and sol-0.3 solvent systems shows a much faster rate of initial Zn-ligand aggregation in sol-0.3 solvent systems followed by a much slower rate of subsequent Zn-ligand rearrangement relative to the DMF solvent systems. This difference in the dynamics between systems employing more polar and less polar solvents was typical across the different dipolar solvents investigated. For example, the Zn-Zn rdf calculated within the 10–50 ns time window appears similar to that calculated within the time window of 0–10 ns in the less polar sol-0.3 solvent systems (see the inset of Fig. 8). In more polar solvent systems, the solvent screening tends to slightly weaken the interactions between Zn-ions and ligands, thereby allowing structural reorganizations to occur, as apparent from the evolution of Zn-Zn rdfs in DMF solvent systems.

Figure S4 in the [supplementary material](#) shows some representative snapshots of the structures observed at the end of typical simulation trajectories (100 ns long) for systems containing sol-0.3, sol-0.4, sol-0.5, sol-0.6, and DMF solvents.

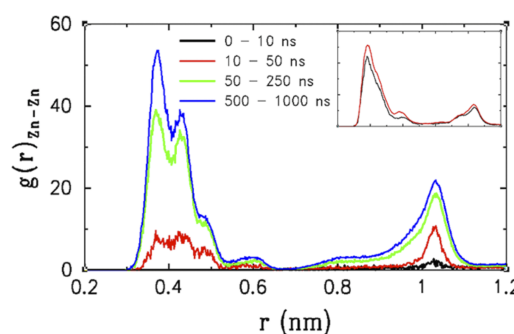


FIG. 8. Evolution of Zn-Zn rdfs, obtained within different time windows, during explicit solvent simulations employing the ECDA(I) Zn-ion model. Black, red, green, and blue lines represent the Zn-Zn rdfs obtained within time windows of 0–10 ns, 10–50 ns, 50–250 ns, and 500–1000 ns, respectively, in DMF solvent. The inset shows the evolution of Zn-Zn rdfs within two time windows [i.e., 0–10 ns (black curve) and 10–50 ns (red curve)] for dipolar solvent (sol-0.3) systems, where the rdf was observed to remain essentially unchanged in subsequent time windows.

Visualization analyses of simulation trajectories for these systems again reveal that less polar solvents (e.g., sol-0.3) aid in the formation of relatively dense, amorphous structures while more polar solvents (e.g., sol-0.55) facilitate formation of more open, ordered structures.

D. Cluster size distributions

1. Solvent influence

To explore further the structural implications of different solvents and different ion models, Zn-Zn and Zn-ligand cluster size distributions were examined. The sizes of various Zn-ion clusters formed during self-assembly processes can be used to investigate and characterize the general features of ordering processes. In this analysis, Zn-ions were considered part of the same cluster if the Zn-Zn distance was $\leq 5 \text{ \AA}$, where this cut-off value was determined from the Zn-Zn radial distribution function for these systems (see Fig. 8). Zn clusters of size 2, 3, 4, and 5 were identified, and the numbers of clusters ($N_{\text{cluster}}^{\alpha}$) of size α were calculated. Figure 9 shows the time evolution of the normalized fraction of clusters ($N_{\text{cluster}}^{\alpha}/N_{\text{max}}^{\alpha}$) for different cluster sizes (i.e., single Zn-ions, size 2, 3, 4, and 5 clusters), where N_{max}^{α} represents the maximum number of clusters possible for the particular cluster size, α . To afford reasonable sampling, these fractions were also averaged over 10 trajectories for each solvent system. A comparison of cluster sizes

for the different dipolar solvent systems reveals that less polar solvents, such as sol-0.3, favor formation of a greater number of large cluster sizes, whereas more polar solvents, such as sol-0.5 and sol-0.6, favor formation of smaller cluster sizes, such as size 2 and 3 clusters. In more polar solvent systems, large cluster sizes tend to appear as more ordered open structures during the later stages of structural evolution due to slower system dynamics.

The behavior of $N_{\text{cluster}}^{\alpha}/N_{\text{max}}^{\alpha}$ for dipolar solvent systems was also compared to that of DMF solvent systems. Because of very slow dynamics in explicit DMF solvent systems compared to the dipolar solvent systems, longer simulations were performed. The behavior of the average Zn-ion cluster size distributions demonstrated by DMF solvent systems was found to most closely resemble to that of the sol-0.5 dipolar solvent systems (and sol-0.55, not shown in Fig. 9). We note that the values of the charge on the oxygen atoms in the DMF model is -0.5 , which corresponds to the site charge in the sol-0.5 dipolar solvent.

While the cluster size distributions of Zn-ion clusters revealed important insights, it is also useful to explore the relationship of cluster size and ligand coordination. Comparison of time evolution of normalized fractions of Zn-ligand clusters ($N_{\text{cluster}}^{\beta}/N_{\text{max}}^{\beta}$) for different cluster sizes (β) in different solvent systems was used for this purpose. These fractions were also averaged over 10 trajectories for each solvent system. A particular Zn-ligand cluster size, β , depends on the number of Zn-ions and the number of surrounding carboxylates, where a cutoff distance of 4 \AA was used for the Zn-ion and carboxylate carbon atom separation. This value was determined from the Zn-carboxylate carbon radial distribution function for these systems. In this way, 1-1, 1-2, and 1-3 clusters (see Fig. S5 in the [supplementary material](#)) that correspond to single Zn-ions coordinated to one, two, and three ligands, respectively, were identified. Similarly, 2-2, 2-3, and 2-4 clusters (see Fig. S6 in the [supplementary material](#)) refer to a pair of Zn-ions coordinated to two, three, and four carboxylate groups, respectively. Consistent with the time evolution behavior of Zn-ion clusters, the number of 1-1, 1-2, and 1-3 clusters was found to decrease with time after a very rapid initial increase for all types of solvent systems, although the extent of decrease depends on the specific solvent employed in that system. Although the 1-2 Zn-ligand cluster was the predominant type of single Zn-ion clusters for all solvent systems, sol-0.6 solvent systems exhibited significant percentages of 1-1 clusters as well (see Fig. S5 in the [supplementary material](#)). The 2-3 and 2-4 Zn-ligand clusters, which appear to be the dominant types of Zn-ligand clusters, were observed to form within ~ 5 ns of simulation in less polar sol-0.3 and sol-0.4 solvent systems and within ~ 20 , ~ 30 , and ~ 100 ns in more polar sol-0.5, sol-0.6, and DMF solvent systems, respectively. The percentage of 2-2 Zn-ligand clusters was found to apparently increase with solvent polarity.

Figure 10 shows average values of the normalized fraction of clusters, $\langle N_{\text{cluster}}^{\alpha}/N_{\text{max}}^{\alpha} \rangle$ and $\langle N_{\text{cluster}}^{\beta}/N_{\text{max}}^{\beta} \rangle$, for different Zn-ion cluster sizes and Zn-ligand cluster sizes, respectively, in continuum solvent simulations with ϵ values of 2, 2.5, and 3. The averaging was performed over 10 trajectories for each system within a time window of 400–500 ns. When the value

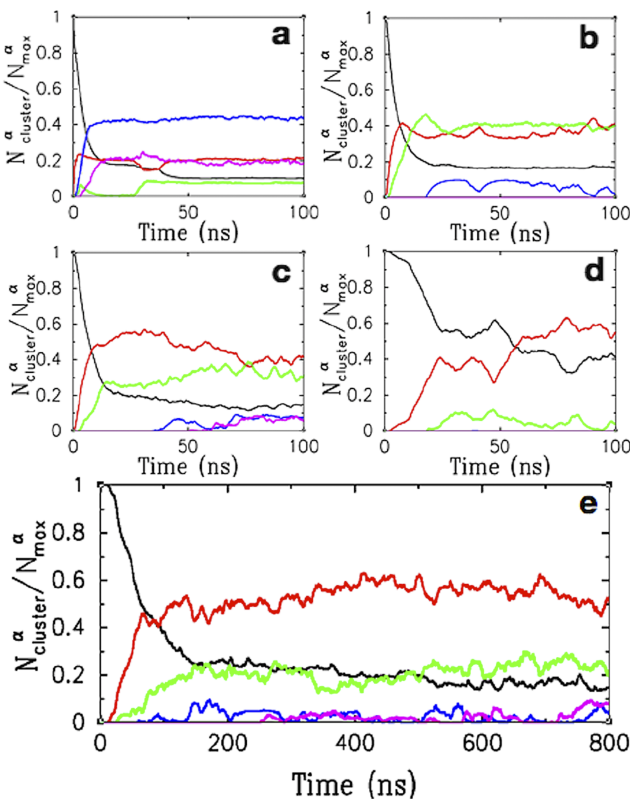


FIG. 9. Solvent dependence of the normalized fraction (by maximum number possible) of Zn-ion clusters ($N_{\text{cluster}}^{\alpha}/N_{\text{max}}^{\alpha}$) for different cluster sizes in simulation systems employing the ECDA(I) Zn-ion model at 450 K. Evolution of $N_{\text{cluster}}^{\alpha}/N_{\text{max}}^{\alpha}$ in sol-0.3, sol-0.4, sol-0.5, sol-0.6, and DMF solvent systems are shown in frames (a)–(e), respectively. The black, red, green, blue, and magenta curves represent single Zn-ions, size 2, size 3, size 4, and size 5 Zn-ion clusters, respectively. We note that for DMF solvent systems, the evolution of $N_{\text{cluster}}^{\alpha}/N_{\text{max}}^{\alpha}$ is shown over a longer time window.

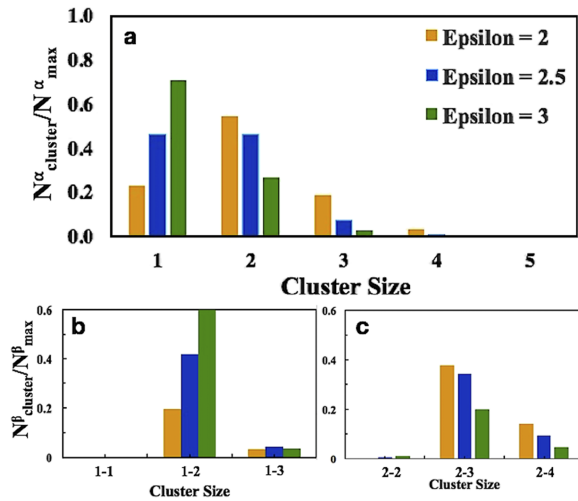


FIG. 10. (a) Dielectric constant dependence of the averaged normalized fraction of Zn-ion clusters, $\langle N_{\text{cluster}}^{\alpha} / N_{\text{max}}^{\alpha} \rangle$, and [(b) and (c)] averaged normalized fraction of Zn-ligand clusters, $\langle N_{\text{cluster}}^{\beta} / N_{\text{max}}^{\beta} \rangle$, for different cluster sizes in continuum solvent systems employing the ECDA(I) Zn-ion model at 450 K. Single Zn-ions coordinated to one, two, and three ligands are denoted as 1-1, 1-2, and 1-3 clusters, respectively. Zn-ion pairs coordinated to two, three, and four ligands are labeled as 2-2, 2-3, and 2-4 clusters, respectively. The yellow, blue, and green bars correspond to $\epsilon = 2, 2.5$, and 3, respectively.

of ϵ increases, the number of single Zn-ions increases, while the number of size 2 and other higher Zn-ion cluster sizes decreases. The single Zn-ion and size 2 clusters primarily form 1-2 and 2-3 type Zn-ligand clusters, respectively, irrespective of the epsilon values in the simulations. A comparison of the cluster size distributions from continuum solvent simulations with those from explicit solvent simulations reveals that continuum solvent simulations with $\epsilon = 2$ exhibit structural characteristics most similar to those found in explicit DMF solvent simulations. For higher dielectric constant values, such as $\epsilon = 3$, the strength of attractive interactions between the Zn-ions and carboxylate groups is weakened, and consequently such systems generally prefer less ordered and lower dimensional structures.

A comparison of the behavior for dipolar solvent and DMF solvent systems, as analyzed through Zn-Zn rdfs and cluster size distributions, consistently demonstrated that sol-0.5 or sol-0.55 dipolar solvents can provide a reasonable solvent medium for exploring self-assembly processes for Zn-carboxylate systems. However, as a consequence of its slightly more polar character, faster rates of structural rearrangement can be achieved through simulations employing the sol-0.55 dipolar solvent model.

2. Comparison of Zn-ion and ligand model behavior

Figure 11 shows average values of the normalized fraction of clusters $\langle N_{\text{cluster}}^{\alpha} / N_{\text{max}}^{\alpha} \rangle$ and $\langle N_{\text{cluster}}^{\beta} / N_{\text{max}}^{\beta} \rangle$ in sol-0.55 solvent systems employing non-bonded(I), CDA(I), and ECDA(I) Zn-ion models. The averaging was performed over 10 trajectories for each system within time windows of 200–300 ns. A comparison of these distributions for the three Zn-ion models reveals that the non-bonded(I) model systems exhibit a strong preference for Zn-ion pair (size-2 cluster) formation, the CDA(I) model system favors formation of larger Zn-ion clusters, i.e., size-3, size-4, and size-5 clusters, and the ECDA(I)

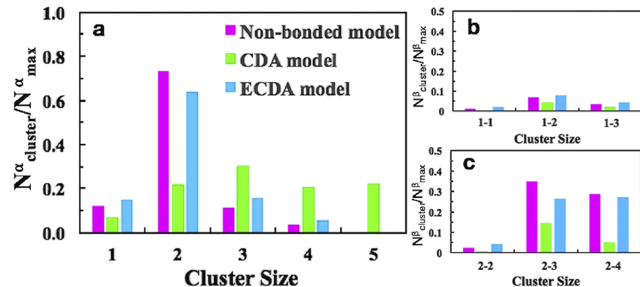


FIG. 11. (a) Zn-ion model dependence of the averaged normalized fraction of Zn-ion clusters, $\langle N_{\text{cluster}}^{\alpha} / N_{\text{max}}^{\alpha} \rangle$, and [(b) and (c)] the averaged normalized fraction of Zn-ligand clusters, $\langle N_{\text{cluster}}^{\beta} / N_{\text{max}}^{\beta} \rangle$, for different cluster sizes in explicit dipolar solvent simulations at 450 K. The magenta, green, and blue bars correspond to the non-bonded(I), CDA(I), and ECDA(I) Zn-ion model systems, respectively.

model system exhibits structural characteristics between these two limits but somewhat closely to the non-bonded(I) model system.

Using an analogous comparison of the average values of normalized fraction of Zn-ion and Zn-ligand clusters (see Fig. S7 in the [supplementary material](#)) in sol-0.55 solvent systems for ECDA Zn(I) (i.e., with net charge of +1.4) and ECDA Zn(II) (i.e., with net charge of +2.0) models, it was found that ECDA Zn(II) model exhibits an increased preference for single Zn-ions and a reduced preference for Zn-ion pairs, relative to the ECDA Zn(I) model. In addition to these Zn-ion models, a coarse-grained (CG) BDC ligand model was also briefly explored (see the [supplementary material](#)).

E. Successful exploration of self-assembly

The above model validation procedure confirmed that the ECDA(I) Zn-ion model performs well in reproducing the experimental MOF-2 structure. Furthermore, the ECDA(I) Zn-ion model combined with a sol-0.55 dipolar solvent medium facilitates the formation of key structural motifs anticipated for this Zn-carboxylate system, for example, as revealed through free energy calculations, while also providing a relatively fast rate of structural rearrangements during MD simulations. To test further if this specific combination of models is appropriate for investigating assembly of appropriate MOF structures during MD simulations, multiple simulation trajectories (250 ns long) were generated for systems containing eight ECDA(I) Zn-ions, four BDC ligands, and four acetate ions in explicit sol-0.55 solvent medium. The behavior of the ECDA(I) Zn-ion model systems was then compared with that from analogous sets of runs employing the CDA(I) and non-bonded(I) Zn-ion models.

Visualization of snapshots from the simulation trajectories for the three sets of systems revealed the following general features (see Fig. S8 in the [supplementary material](#)): 1. The non-bonded(I) model exhibits a strong preference for formation of triangular structures consisting mostly of Zn-ion pairs; 2. the ECDA(I) model favors formation of a variety of structures including triangular and square (MOF-2 like) arrangements; and 3. the CDA(I) model exhibits a strong tendency to form larger Zn-ion clusters or aggregates that are bridged by carboxylate ligands in chain-like structural arrangements. Figure 12 presents several snapshots from one of the

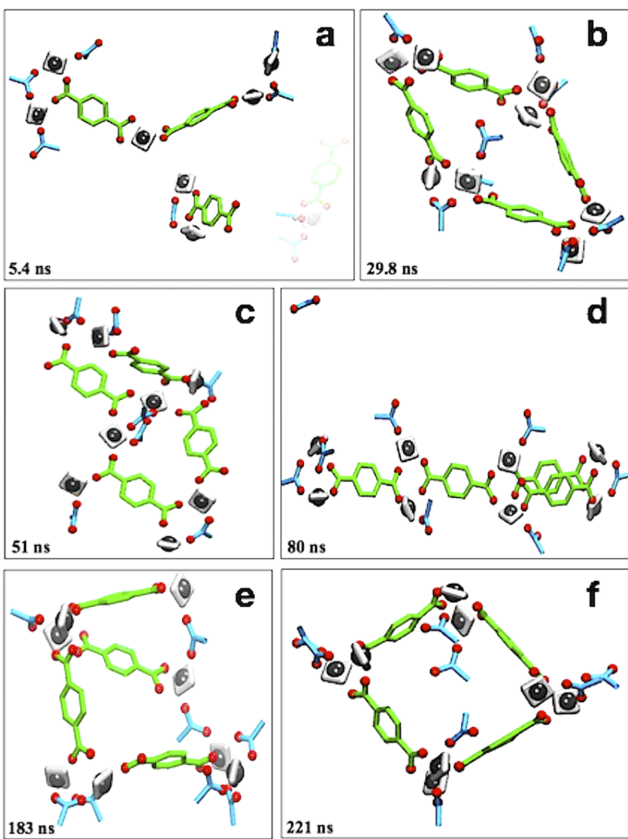


FIG. 12. Snapshots of an ECDA(I) Zn-ion system at various stages of the self-assembly process, and featuring a MOF-2-like square arrangement, as observed during one of the simulation trajectories in explicit dipolar solvent simulations at 450 K. The time index for each of the frames (a)–(f) is provided. The Zn-ions, BDC ligands, and acetate ions are colored as gray, green, and cyan, respectively, and solvents molecules are not shown for visual clarity.

ECDA(I) system trajectories that successfully assembled a MOF-2 like square arrangement within 250 ns. This particular trajectory also demonstrates an important aspect of the self-assembly process, namely, reversibility. A (roughly) square arrangement was observed to form within ~30 ns of simulation time [see Fig. 12(b)], however unmaking and reassembly of a superior structure was achieved within the 250 ns simulation.

Both ECDA(I) and non-bonded(I) systems demonstrate a preference for formation of Zn-ion pairs and 2-3 Zn-ligand clusters although the preference is more pronounced in systems using the latter Zn-ion model. Systems with the CDA(I) model exhibit a preference for polymeric structural entities, where key structural motifs such as Zn-ion pairs and 2-3 Zn-ligand clusters are less likely to appear. Hence, the CDA(I) model does not appear to represent a suitable model for exploring self-assembly processes in this archetypal Zn-carboxylate MOF system. While there are similarities in the behaviors of the ECDA(I) and non-bonded(I) Zn-ion systems, a prominent structural difference was found through analysis of average coordination numbers of carboxylate oxygen atoms within the immediate coordination shell of the Zn-ions (see Fig. S8 in the [supplementary material](#)). On average, three carboxylate oxygens were found for the ECDA(I) model, while only two carboxylate oxygens were calculated for the non-bonded(I) Zn-ion model within the immediate coordination shell of the

Zn-ions. Increased strength of electrostatic interactions leads to a stronger binding of carboxylate oxygens around Zn-ions in systems with the ECDA(I) model compared to that in systems with the non-bonded(I) model.

The appearance of some of the major structures during simulations of self-assembly can be reasonably attributed to thermodynamic factors, for example, those identified through calculations of relative free energies. For example, the PWC-3 motif (motif E, see Fig. 7) has been identified as a free energy minimum structure for systems with the ECDA(I) Zn-ion model. Thus, formation of a large number of PWC-3 motifs in systems employing the ECDA(I) Zn-ion model appears due to its relative stability. However, trimeric Zn-ion clusters and monomeric Zn-complexes also appear during structural evolution in these systems and can be considered as kinetic products.

IV. CONCLUSION

In this study, we have examined and explicitly compared the behavior of different Zn-ions and solvent models to identify suitable model combinations to explore self-assembly processes in an archetypal Zn-carboxylate system. The ECDA(I) Zn-ion model can be effectively used to investigate relatively long time-scale ordering events. Notably, the ECDA(I) Zn-ion model is capable of reproducing well the structural features of a MOF-2 structure, a commonly occurring MOF structure observed in Zn-carboxylate systems. Also, it was demonstrated that the ECDA(I) Zn-ion model supports the assembly of key structural motifs anticipated for this archetypal Zn-carboxylate system. Investigation of different solvent behaviors demonstrated that simple solvent models (such as sol-0.55 dipolar solvent) appear to be a reasonable compromise for exploring relatively longer time scale ordering processes in explicit solvent simulations. Thus, a combination of the ECDA(I) Zn-ion model, a sol-0.55 dipolar solvent model, and BDC ligands in explicit solvent simulations afford a reasonable choice for probing longer time-scale and larger length-scale ordering events associated with the self-assembly processes for an archetypal Zn-carboxylate system. The successful application of these models to the elucidation of the self-assembly mechanisms during the earlier stages of MOF self-assembly process has very recently appeared.⁶⁶

An important lesson learnt through this study is that models should be carefully chosen for MOF self-assembly studies, as such choices can, for example, impart specific coordination characteristics to metal-ions. We have also demonstrated that simplified solvent models (e.g., continuum solvents), while being computationally attractive, should be used with considerable care to ensure that they reasonably reproduce the behavior of explicit solvent systems. The models investigated in this study (or variants of these) can, in principle, be used to study self-assembly processes in similar MOF systems, such as other Zn-carboxylate MOFs. Currently, we are investigating the Zn-ligand potentials of mean force in an effort to further explore the impacts of key model features with the goal of improving the performance of the ECDA Zn-ion model.

SUPPLEMENTARY MATERIAL

See [supplementary material](#) for details of the models employed, including dielectric constants of dipolar solvent models, a preliminary comparison of a coarse-grain ligand model, and numerical values obtained from free energy calculations. Several additional figures are also presented.

ACKNOWLEDGMENTS

We are grateful for the financial support of the Natural Sciences and Engineering Research Council of Canada (Grant No. RGPIN-2016-03845) and the Canadian Foundation for Innovation. We also acknowledge computational resources made available via WestGrid (www.westgrid.ca) and Compute Canada (www.computecanada.ca).

- ¹L. Xie, G. R. Smith, X. Feng, and R. Schwartz, *Biophys. J.* **103**, 1545 (2012).
- ²D. C. Rappaport, *Phys. Rev. E* **86**, 051917 (2012).
- ³B. Chen and R. Tycko, *Biophys. J.* **100**, 3035 (2011).
- ⁴J. M. Grime and G. A. Voth, *Biophys. J.* **103**, 1774 (2012).
- ⁵T. Carpenter, P. J. Bond, S. Khalid, and M. S. P. Sansom, *Biophys. J.* **95**, 3790 (2008).
- ⁶K. A. Scott, P. J. Bond, A. Iveta, A. P. Chetwynd, S. Khalid, and M. S. Sansom, *Structure* **16**, 621 (2008).
- ⁷A. A. Skjevik, B. D. Madej, C. J. Dickson, C. Lin, K. Teigen, R. C. Walker, and I. R. Gould, *Phys. Chem. Chem. Phys.* **18**, 10573 (2016).
- ⁸A. H. de Vries, A. E. Mark, and S. J. Marrink, *J. Am. Chem. Soc.* **126**, 4488 (2004).
- ⁹S. Esteban-Martin and J. Salgado, *Biophys. J.* **92**, 903 (2007).
- ¹⁰D. Pogor, W. F. van Gunsteren, and A. E. Mark, *J. Comput. Chem.* **31**, 1117 (2010).
- ¹¹S. Khalid, P. J. Bond, J. Holyoake, R. W. Hawtin, and M. S. P. Sansom, *J. R. Soc., Interface* **5**(Supp. 3), 241 (2008).
- ¹²P. J. Bond, J. Holyoake, A. Iveta, S. Khalid, and M. S. Sansom, *J. Struct. Biol.* **157**, 593 (2007).
- ¹³S. J. Marrink and A. E. Mark, *J. Am. Chem. Soc.* **125**, 15233 (2003).
- ¹⁴W. Shinoda, R. DeVane, and M. L. Klein, *J. Phys. Chem. B* **114**, 6836 (2010).
- ¹⁵N. Thota, Z. Luo, Z. Hu, and J. Jiang, *J. Phys. Chem. B* **117**, 9690 (2013).
- ¹⁶S. Liang and P. G. Kusalik, *Chem. Sci.* **2**, 1286 (2011).
- ¹⁷J. Vatamanu and P. G. Kusalik, *Phys. Chem. Chem. Phys.* **12**, 15065 (2010).
- ¹⁸M. R. Walsh, G. T. Beckham, C. A. Koh, E. D. Sloan, D. T. Wu, and A. K. Sum, *J. Phys. Chem. C* **115**, 21241 (2011).
- ¹⁹E. J. Wallace and M. S. Sansom, *Nanotechnology* **20**, 045101 (2009).
- ²⁰M. Luo and L. L. Dai, *J. Phys.: Condens. Matter* **19**, 375109 (2007).
- ²¹G. Srinivas and M. L. Klein, *Nanotechnology* **18**, 205703 (2007).
- ²²H. C. Zhou and S. Kitagawa, *Chem. Soc. Rev.* **43**, 5415 (2014).
- ²³H. C. Zhou, J. R. Long, and O. M. Yaghi, *Chem. Rev.* **112**, 673 (2012).
- ²⁴M. P. Suh, H. J. Park, T. K. Prasad, and D.-W. Lim, *Chem. Rev.* **112**, 782 (2012).
- ²⁵J. Liu, L. Chen, H. Cui, J. Zhang, L. Zhang, and C.-Y. Su, *Chem. Soc. Rev.* **43**, 6011 (2014).
- ²⁶T. Davic and C. Serre, *Chem. Soc. Rev.* **43**, 6097 (2014).
- ²⁷C. Pagis, M. Ferbinteanu, G. Rothenberg, and S. Tanase, *ACS Catal.* **6**, 6063 (2016).
- ²⁸M. Eddaoudi, D. B. Moler, H. Li, B. Chen, T. M. Reineke, M. O'Keeffe, and O. M. Yaghi, *Acc. Chem. Res.* **34**, 319 (2001).
- ²⁹O. M. Yaghi, M. O'Keeffe, N. W. Ockwig, H. K. Chae, M. Eddaoudi, and J. Kim, *Nature* **423**, 705 (2003).
- ³⁰D. J. Tranchemontagne, J. L. Mendoza-Cortés, M. O'Keeffe, and O. M. Yaghi, *Chem. Soc. Rev.* **38**, 1257 (2009).
- ³¹M. Shoaei, M. W. Anderson, and M. P. Attfield, *Angew. Chem., Int. Ed.* **47**, 8525 (2008).
- ³²J. A. Rood, W. C. Boggess, B. C. Noll, and K. W. Henderson, *J. Am. Chem. Soc.* **129**, 13675 (2007).
- ³³M. Li and M. Dincă, *Chem. Mater.* **27**, 3203 (2015).
- ³⁴G. Férey, M. Haouas, T. Loiseau, and F. Taulelle, *Chem. Mater.* **26**, 299 (2014).
- ³⁵S. Surblé, F. Millange, C. Serre, G. Férey, and R. I. Walton, *Chem. Commun.* **0**, 1518 (2006).
- ³⁶M. G. Goesten, E. Stavitski, J. Juan-Alcañiz, A. Martínez-Joaristi, A. V. Petukhov, F. Kapteijn, and J. Gason, *Catal. Today* **205**, 120 (2013).
- ³⁷M. G. Goesten, P. C. M. M. Magusin, E. A. Pidko, B. Mezari, E. J. M. Hensen, F. Kapteijn, and J. Gason, *Inorg. Chem.* **53**, 882 (2014).
- ³⁸R. E. Morris, *ChemPhysChem* **10**, 327 (2009).
- ³⁹D. C. Rappaport, *Phys. Rev. E* **70**, 051905 (2004).
- ⁴⁰G. Srinivas and J. W. Pitera, *Nano Lett.* **8**, 611 (2008).
- ⁴¹A. Y. Shih, A. Arkhipov, P. L. Freddolino, S. G. Sligar, and K. Schulten, *J. Phys. Chem. B* **111**, 11095 (2007).
- ⁴²G. Srinivas, J. C. Shell, S. O. Nielsen, D. E. Discher, and M. L. Klein, *J. Phys. Chem. B* **108**, 8153 (2004).
- ⁴³J. Anwar and P. K. Boateng, *J. Am. Chem. Soc.* **120**, 9600 (1998).
- ⁴⁴S. Auer and D. Frenkel, *Nature* **409**, 1020 (2000).
- ⁴⁵R. H. Stote and M. Karplus, *Proteins* **23**, 12 (1995).
- ⁴⁶J. Åqvist, *J. Mol. Struct.: THEOCHEM* **256**, 135 (1992).
- ⁴⁷R. D. Hancock, *Acc. Chem. Res.* **23**, 253 (1990).
- ⁴⁸A. Vedani and D. W. Huhta, *J. Am. Chem. Soc.* **112**, 4759 (1990).
- ⁴⁹Y. P. Pang, K. Xu, J. E. Yazal, and F. G. Prendergast, *Protein Sci.* **9**, 1857 (2000).
- ⁵⁰Y. P. Pang, *J. Mol. Model.* **5**, 196 (1999).
- ⁵¹P. Oelschlaeger, M. Klahn, W. A. Beard, S. H. Wilson, and A. Warshel, *J. Mol. Biol.* **366**, 687 (2007).
- ⁵²J. Åqvist and A. Warshel, *J. Am. Chem. Soc.* **112**, 2860 (1990).
- ⁵³F. Lin and R. X. Wang, *J. Chem. Theory Comput.* **6**, 1852 (2010).
- ⁵⁴U. Ryde, *Proteins* **21**, 40 (1995).
- ⁵⁵F. Duarte, P. Bauer, A. Barrozo, B. A. Amrein, M. Purg, J. Åqvist, and S. C. L. Kamerlin, *J. Phys. Chem. B* **118**, 4351 (2014).
- ⁵⁶M. Yoneya, T. Yamaguchi, S. Sato, and M. Fujita, *J. Am. Chem. Soc.* **134**, 14401 (2012).
- ⁵⁷M. Yoneya, S. Tsuzuki, and M. Aoyagi, *Phys. Chem. Chem. Phys.* **17**, 8649 (2015).
- ⁵⁸H. Li, M. Eddaoudi, T. L. Groy, and O. M. Yaghi, *J. Am. Chem. Soc.* **120**, 8571 (1998).
- ⁵⁹H. Li, C. E. Davis, T. L. Groy, D. G. Kelley, and O. M. Yaghi, *J. Am. Chem. Soc.* **120**, 2186 (1998).
- ⁶⁰G. Gilera and J. W. Steed, *Chem. Commun.* **20**, 1563 (1999).
- ⁶¹S.-Y. Yang, L.-S. Long, R.-B. Huang, and L.-S. Zheng, *Main Group Met. Chem.* **25**, 329 (2002).
- ⁶²M. Edgar, R. Mitchell, A. M. Z. Slawin, P. Lightfoot, and P. A. Wright, *Chem. - Eur. J.* **7**, 5168 (2001).
- ⁶³S. I. Vagin, A. K. Ott, and B. Rieger, *Chem. Ing. Tech.* **79**, 767 (2007).
- ⁶⁴S. M. Hawxwell, H. Adams, and L. Brammer, *Acta Crystallogr., Sect. B: Struct. Sci.* **62**, 808 (2006).
- ⁶⁵S. Y. Yang, L. S. Long, R. B. Huang, L. S. Zheng, and S. W. Ng, *Acta Crystallogr., Sect. E: Struct. Rep. Online* **61**, m1671 (2005).
- ⁶⁶D. Biswal and P. G. Kusalik, *ACS Nano* **11**, 258 (2017).
- ⁶⁷T. Dudev and C. Lim, *J. Am. Chem. Soc.* **124**, 6759 (2002).
- ⁶⁸J. Koca, C. G. Jhan, R. C. Rittenhouse, and R. L. Ornstein, *J. Comput. Chem.* **24**, 368 (2003).
- ⁶⁹Y. L. Li, Y. Mei, D. W. Zhang, D. Q. Xie, and J. Z. H. Zhang, *J. Phys. Chem. B* **115**, 10154 (2011).
- ⁷⁰W. L. Jorgensen, D. S. Maxwell, and J. Tirado-Rives, *J. Am. Chem. Soc.* **118**, 11225 (1996).
- ⁷¹J. Weeks, D. Chandler, and H. Andersen, *J. Chem. Phys.* **54**, 5237 (1971).
- ⁷²S. Pronk, S. Pälli, R. Schulz, P. Larsson, P. Bjelkmar, R. Apostolov, M. R. Shirts, J. C. Smith, P. M. Kasson, D. van der Spoel, B. Hess, and E. Lindahl, *Bioinformatics* **29**, 845 (2013).
- ⁷³T. Darden, D. York, and L. Pedersen, *J. Chem. Phys.* **98**, 10089 (1993).
- ⁷⁴H. J. C. Berendsen, J. P. M. Postma, W. F. van Gunsteren, A. DiNola, and J. R. Haak, *J. Chem. Phys.* **81**, 3684 (1984).
- ⁷⁵B. Hess, H. Bekker, H. J. C. Berendsen, and J. G. E. M. Fraaije, *J. Comput. Chem.* **18**, 1463 (1997).
- ⁷⁶P. Kollman, *Chem. Rev.* **93**, 2395 (1993).
- ⁷⁷S. Bureekaew, S. Amirjalayer, and R. Schmid, *J. Mater. Chem.* **22**, 10249 (2012).
- ⁷⁸A. Erxleben, *Coord. Chem. Rev.* **246**, 203 (2003).
- ⁷⁹J. P. Larentzos and L. J. Criscenti, *J. Phys. Chem. B* **112**, 14243 (2008).